# Energy Efficient Future Generation Electronics Based on Strongly Correlated Electron Systems


**Abhijit Chanda, Sudipta Goswami and Dipten Bhattacharya**

**Abstract** Three major developments in three decades are quietly changing the whole spectrum of 'electronics' (as it is conventionally known) making it ready for a major revolution. At the heart of this lies the 'electronics based on strongly correlated electron systems'. The broad canvass of 'strongly correlated electron systems'—especially the ones assuming importance for future generation electronics—covers primarily transition metal ion based complex oxide compounds exhibiting superconductivity at a record high temperature (cuprate superconductors); gigantic change in electrical resistivity under tiny magnetic field (CMR manganites); and coexisting ferroelectric and magnetic orders within a single phase with an extraordinary cross-coupling (multiferroics). Thanks to these developments, apart from charge of an electron, its spin and orbital degrees of freedom are now being shown to offer tremendous manoeuvrability for developing not just electronic but spintronic and orbitronic devices as well. Larger coherence length and stability of spin and orbital spectra can be exploited for bringing functionalities hitherto unknown. Using up and down spins and different patterns of orbital occupancy of the electrons, it is now possible to design and develop spintronic and even orbitronic devices by exploiting esoteric effects such as spin-transport, spin-tunnelling, spin-Hall, spin-Seebeck or switching of orbital orders under optical illumination. These nanoscale devices are energy efficient and ultra-sensitive. They are expected to perform more complex jobs in a vast arena which includes even bio-electronics.

A. Chanda
Department of Mechanical Engineering, Jadavpur University,
Kolkata 700032, India
e-mail: abhijitchanda.biomed@gmail.com

S. Goswami
Department of Solid State Physics, Indian Association for the Cultivation
of Science, Kolkata 700032, India
e-mail: drsudiptagoswami@gmail.com

D. Bhattacharya (✉)
Nanostructured Materials Division, CSIR-Central Glass and Ceramic
Research Institute, Kolkata 700032, India
e-mail: dipten@cgcri.res.in



S. De et al. (eds.), *Sustainable Energy Technology and Policies*,
Green Energy and Technology, https://doi.org/10.1007/978-981-10-8393-8_18

In this article, we introduce the area of strongly correlated electron systems and explore the advancements already made and possibilities emerging in developing future generation electronic-spintronic-orbitronic devices based on complexities which till now stubbornly defied complete understanding in spite of intense efforts worldwide—a classic example of which is the mechanism of high temperature cuprate based superconductors.

## 1 Introduction

With the discovery of superconductivity at a record high temperature of $\sim$35 K in Ba-doped $La_2CuO_4$ in 1986 [1], a new chapter in the area of oxide electronic materials began. The importance of $ABO_3$ perovskite systems and its higher order derivatives including layered Aurivillus phase, double perovskite $A_2B_2O_6$ or Ruddlesden-Popper systems $A_3B_2O_7$ in yielding complex functionalities within the domain of electronic, magnetic, and optical properties started unfolding slowly. After three decades since 1986 and many seminal discoveries in the meantime with this class of compounds, the situation seems well poised to change the entire area of 'electronics'—as it is conventionally known since the era of Si-based devices—though full scale commercial usage is still a few years away. Apart from the 'charge' of an electron, 'spin' and 'orbital' degrees of freedom are also now accessible for utilization in new generation 'electronic' devices. Three decades saw development of three new areas: (i) high temperature superconductivity [2], (ii) colossal magnetoresistivity [3], and (iii) multiferroicity [4]. The high temperature copper oxide based superconductors were projected to revolutionize the power transmission, storage, and generation besides having large scale applications in electronic circuitry as fault current limiters and Joesphson devices. The gigantic magnetoresistivity (orders of magnitude drop in resistivity under a magnetic field) in perovskite manganites was found to be promising for applications such as magnetic read/write heads allowing enormous jump in the data storage density, magnetic memories, other field-effect devices, and even in detection of infrared radiation. The multiferroics, on the other hand, with coexisting ferroelectric and magnetic phases and a cross-coupling between the order parameters offer an additional handle for writing the memory devices electrically and reading magnetically which, in turn, reduces the power consumption drastically while enhancing the storage density of a memory device. The era of new generation electronic, spintronic, optoelectronic, optospintronic, or orbitronic devices is about to begin. These perovskites and their derivative systems possess complex crystallographic and electronic structure and often described as 'strongly correlated electron' systems. In spite of diversity in them, there are certain commonalities as well.

It is important to point out here that much of the new generation electronic and spintronic devices such as bipolar switches, filters, spin valves, memories, read/write heads etc. would possibly be developed from even metallic magnetic

multilayers (e.g., ferromagnetic layers sandwiching a nonmagnetic layer) and dilute magnetic semiconductors [5] which do not fall into the category of 'strongly correlated electron systems'. We keep them out of our discussion as we focus on the energy efficient devices based on 'strongly correlated electron' systems alone.

In this article, we shall first introduce the physics of these complex oxides and underline how they are different and more complex from conventional metal, semimetal, semiconductor, and insulator and how this complexity can be fully exploited for novel applications. We shall then highlight the advancements made in real-life device fabrications using this class of compounds.

## 2 Strongly Correlated Electron Systems

Based on the electronic band structure and electrical properties, the entire class of materials can be categorized as metal, semiconductor, and insulator. While metals do not possess a gap in the electron band near Fermi level, semiconductor and insulators contain small to large band gaps of the order of even few eV. The Fermi energy ($E_F$) or Fermi velocity ($v_F$) is orders of magnitude higher than the lattice Debye energy ($E_D$). The electron-phonon coupling is generally weak. The effective mass (m*) of free electrons at the Fermi surface in a metal is comparable with free electron mass ($m_e$), i.e., $m^* \approx m_e$. The Coulomb interaction among the electrons is much smaller than the other energy scales such as kinetic and electron-phonon interaction energy. Therefore, it is treated as a perturbation leading to negligible renormalization of the effective electron parameters such as velocity, mass, momentum, energy etc. The situation changes completely in a certain class of compounds where the Fermi energy is an order of magnitude smaller and the density of states at the Fermi level is large. The electron-electron Coulomb interaction energy becomes no longer negligible. These compounds are categorized as 'strongly correlated electron systems'. The effective mass of an electron (m*) in these cases turns out be varying from $\sim 10\ m_e$ to $\sim 1000\ m_e$. The perovskites and their derivatives—pointed out above—containing transition metal ions belong to this 'strongly correlated electron' class and as such form the heart of the new generation electronic devices. This strong correlation among the electrons gives rise to novel phenomena such as metal-insulator transition, colossal magnetoresistivity, and even superconductivity at a very high temperature [6]. The onsite electron-electron repulsion appears to be primarily responsible for the development of gap in the band structure near Fermi level (Fig. 1) which, in turn, leads to insulating ground state. Interestingly, one electron band structure in the absence of Coulomb interaction predicts metallic state. This Mott insulating state undergoes metallic transition upon doping which creates mobile charge carriers for hopping from site to site. Instead of band conduction, these systems, therefore, exhibit hopping conduction with formation of polarons. The polarons form due to the change in polarization of the ion sites in presence of hopping charge carriers. The properties such as electrical resistivity, thermoelectric power, specific heat, thermal

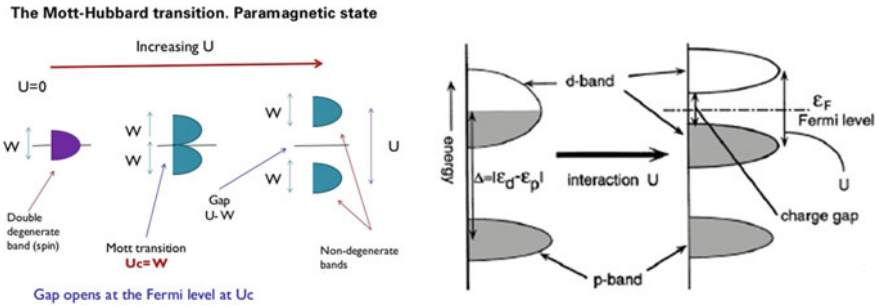


**Fig. 1** The schematic of band gap at the Fermi level as a result of electron correlation (i.e., Coulomb repulsion)

conductivity, optical conductivity etc. exhibit completely different pattern and dependence on parameters such as temperature, pressure, magnetic field or optical pulse is nontrivial. The electrons (better called quasiparticles as the mass, momentum, energy etc. vary around their mean values) of these systems with large renormalization of the parameters such as mass, momentum, velocity, energy cannot be described by conventional Fermi liquid formalisms. They are described by different non-Fermi liquid theories [7]. In such systems, the Fermi surface deviates from the conventional spherical shape and becomes more anisotropic with even rather blurred edges. An important aspect of the strongly correlated electron systems is the interplay among different degrees of freedom of the electrons—such as charge, spin, and orbital—with the lattice. This interplay, in fact, gives rise to the formation of different ordered pattern of the charge, spin, and orbital degrees of freedom of the electrons. Another important feature of this class of materials is the intrinsic structural and/or electronic phase segregation and consequent coexistence of ordered and disordered or metal and insulator phases. This enormous complexity makes this class of materials an extremely fertile ground for observing and/or engineering newer phenomena. We shall now discuss the essential physics of the cuprate superconductors, magnetoresistive manganites, and multiferroics.

## *2.1 Cuprate Superconductors*

We shall restrict our discussion within three families of cuprate superconductors: (i) $YBa_2Cu_3O_{7-x}$ (YBCO), (ii) $Bi_2Sr_2CaCu_2O_8$ (BSCCO2212), and (iii) $Bi_2Sr_2Ca_2Cu_3O_{10}$ (BSCCO2223). We leave out the Tl- and Hg-based compounds because of their toxicity and consequent smaller chance of finding real-life applications. The salient features of the cuprate superconductors are given here: (i) the superconducting transition temperatures $T_C$ (below which electrical resistivity becomes zero and magnetic flux is excluded from the bulk of the sample) for these compounds are $\sim$90 K [8], $\sim$85 K [9], and $\sim$110 K [10], respectively;

(ii) above $T_C$, they exhibit metallic resistivity pattern though the normal state resistivity of these systems is quite high (of the order of few milli-Ohm.cm); the conductivity ($\sigma$) is smaller than even Mott's minimum metallic conductivity $\sigma_m$ ($\sim a/l_{mfp}$; $l_{mfp}$ is the electron mean free path and $a$ is the lattice constant) [11]; (ii) the normal state resistivity ($\rho$) follows linear temperature (T) dependence (i.e., $\rho \sim T$) which is unusual for a metal and signifies non-Fermi liquid character of the electron fluid at the Fermi level; (iii) linear T dependence of the normal state $\rho$ influences the optical conductivity $\sigma_1(\omega)$ across a large frequency ($\omega$) range up to microwave frequency; in fact, $\sigma(\omega)$ is given by $\rho(T)$ and the Drude conductivity spectrum; of course, while YBCO system exhibits large frequency dependence of $\sigma_1$ in the low temperature range, it is absent in BSCCO system [12]; (iv) the thermoelectric power (S) follows $\sim A + BT$ temperature dependence in the high temperature region; (v) large anisotropy with conducting Cu–O layers sandwiched between charge-reservoir layers comprising of other elements of the compound; the anisotropy depends on the number of Cu–O layers in the unit cell; while YBCO and BSCCO contain two Cu–O layers, BSCCO2223 contains three layers (Fig. 2); anisotropy, accordingly, in creases from $\sim 10^2$ in YBCO to $\sim 10^5$ in BSCCO2223; (vi) transition temperature $T_C$ depends strongly on the doping level (x) of the Cu–O plane; it increases initially with the increase in 'x' and then reaches maximum and finally drops off (Fig. 2); three regions are marked as 'underdoped', 'optimally doped', and 'overdoped'; $T_C$ fits $T_C/T_{C,max} \sim 1 - 82.6(x - 0.16)^2$ relation well [13]; (vii) in almost all the cases of the cuprate superconductors, the parent undoped compound is antiferromagnetic and insulator; doping induces spin fluctuations and breaks the long-range magnetic order and drives insulator to metal transition; eventually, at a critical doping level $x = x_C$, the superconductivity sets in; prevalence of spin fluctuations is considered a vital ingredient for inducing pairing of electrons necessary for superconductivity to set in; (viii) a pseudogap opens up far above $T_C$ in the electron spectrum (which could as well be a gap in the spin spectrum) of the cuprate superconductors whose presence is reflected in NMR data,

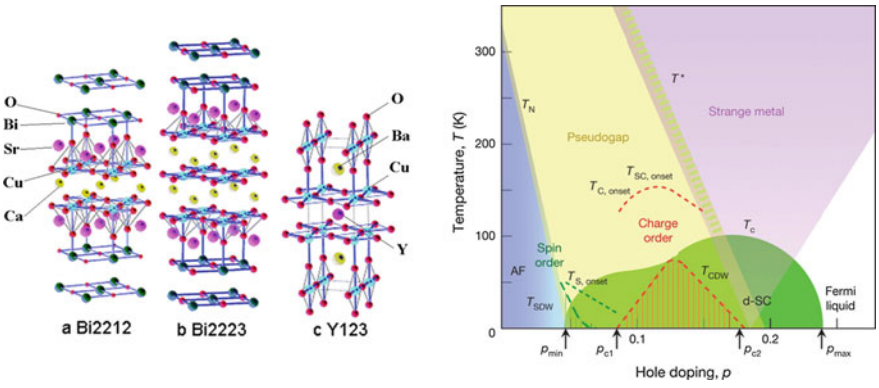


**Fig. 2** The crystallographic structures of **a** BSCCO2212, **b** BSCCO2223, and **c** YBCO; right panel shows the generic electronic phase diagram of the cuprate superconductors

infrared reflectivity, dc resistivity, thermoelectric power etc.; (ix) the paired electrons assume anisotropic d-wave symmetry resulting from higher order spin triplet formation; (x) importantly, the magnetic phase diagram is extremely complex [14] comprising of vortex solid, glass, and liquid phases in different regions of the field (H)—temperature (T) diagram; giant vortex creeping [15] across a wide region of the magnetic phase diagram—which gives rise to finite electrical resistivity by destroying superconductivity—actually is responsible for rather limited application potential for these cuprate superconductors.

## 2.2 *Colossal Magnetoresistive Manganites*

Within a few years of the discovery of cuprate superconductors, another surprising discovery was made in 1992 in $ABO_3$ type compounds $RMnO_3$ (R = La, Pr, Nd, Sm) (Fig. 3). In a thin film of $La_{0.7}Ca_{0.3}MnO_3$, a gigantic decrease in electrical resistivity (of the order $\sim 10^6$) was observed under a magnetic field of few tesla [16]. Such a large drop in resistivity under magnetic field, i.e., magnetoresistivity was unprecedented. In the subsequent years, the full spectrum of the properties and phase diagram was explored. This class of compounds provides a classic playground to demonstrate close relationship between magnetic and electrical properties. While antiferromagnetic order gives rise to insulating behaviour, ferromagnetism is found to be concomitant to metallicity. The salient features of this class of compounds are given here. (i) The parent $RMnO_3$ (R = La, Pr, Nd, Sm) compound is antiferromagnetic and insulating; the antiferromagnetic order is A-type where spins are aligned ferromagnetically within a Mn-O plane and antiferromagnetically across the plane; depending on the average R-site radius $\langle r_R \rangle$, the phase diagram and the transition temperatures change dramatically; this offers a tool for tuning the properties [17]; (ii) with the increase in doping by alkali ions such as $Ca^{2+}$, $Sr^{2+}$, $Ba^{2+}$ at the R-site, the antiferromagnetic order melts and antiferromagnetic to ferromagnetic and insulator to metallic transition sets in (Fig. 3); the

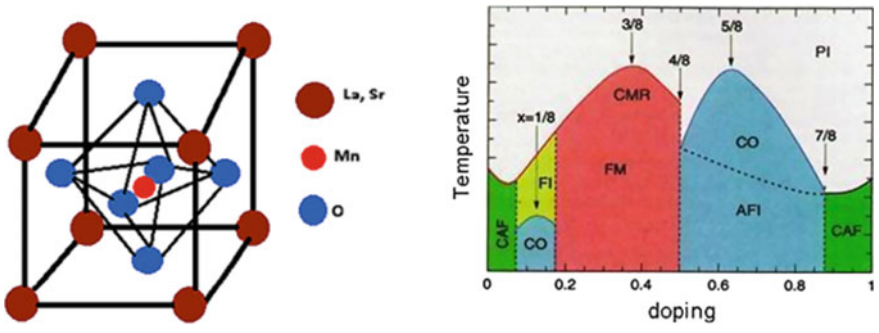


**Fig. 3** The crystallographic structure of perovskite $LaMnO_3$; right panel shows the generic electronic phase diagram of the manganites

critical doping level $x_C$ varies within $\sim$0.17–0.20; higher the $\langle r_R \rangle$ smaller is the $x_C$; the ferromagnetic and metallic behaviour is governed by double exchange interaction across $Mn^{3+}$–$O^{2-}$–$Mn^{3+}$ bonds where exchange coupling between the spins at the Mn sites develops as a result of hopping of electrons from site to site; (iii) the entire electronic phase diagram comprises of, primarily, antiferromagnetic insulating, ferromagnetic metallic, and, again, antiferromagnetic insulating phases as the doping level 'x' increases from zero to 1.0. The structure of antiferromagnetic order, of course, changes from low doping to higher doping range—from A-type (mentioned above) to C-type (one-dimensional spin chain), to CE-type (two-dimensional zigzag), to E-type (spin chain with rotation), and eventually to G-type (three-dimensional antiferromagnetic); (iv) the intermediate doping range $x \sim 0.2$–0.4 exhibits the ferromagnetic and metallic properties where colossal magnetoresistivity is also observed; (v) this class of materials also exhibit, at different regions of the phase diagram, real-space ordering of charge and orbital degrees of freedom; the charge/orbital order too assumes different patterns such as C, CE, or E type [18]; (vi) importantly, like magnetic order, the change/orbital order too melts under different external stimulations such as magnetic field, electric field, and optical pulses [19] and gives rise to gigantic change in the physical properties such as electrical resistivity, magnetization, thermal and optical properties; (vii) an important aspect of these manganites is the intrinsic structural and/or electronic phase segregation which leads to the formation of coexisting metallic and insulating phases; the colossal magnetoresistivity was shown as outcome of percolation of the metallic phase under magnetic field in an effective medium type theory.

## *2.3 Multiferroics*

Although first observed [20] in early 1960s, the resurgence of the area of multiferroics took place in the new millennium because of two important observations—one theoretical and another experimental. The multiferroics harness different ferro orders such as '(anti)ferroelastic', '(anti)ferroelectric', and '(anti)ferromagnetic' orders within a single phase. More importantly, there exists a cross-coupling among the order parameters which makes polarizing the sample by magnetic field and vice versa possible. In 2000, based on theoretical calculations it was argued [21] that a transition metal ion with partially filled 3d levels cannot give rise to covalency driven instability necessary for structural off-centering, i.e., ferroelectricity. This is because of centrosymmetric distortion (Jahn-Teller) associated with magnetic ions. Only $3d^0$ ions (observed in $Ti^{4+}$ in $BaTiO_3$ or $PbTiO_3$) can give rise to off-centric distortion. As a result of this, multiferroic compounds are rare in nature. The ferroelectric instability arises in a different sublattice in compounds which exhibit coexisting ferroelectric and magnetic phases. This observation triggered renewed search for new set of compounds with such characteristics. In 2003, another group showed [22] in an experimental work that epitaxial thin film of $BiFeO_3$—a compound known to be multiferroic since early 1960s—does exhibit large ferroelectric

polarization and magnetization at room temperature. In fact, the ferroelectric and magnetic transition temperatures are ~1103 and ~650 K, respectively. This work initiated rigorous attempts to explore and exploit the multiferroicity in $BiFeO_3$ in various forms—single crystal, epitaxial thin films with a design to observe host of different characteristics, and nanosized particles. Given the knowledgebase generated so far, it appears that $BiFeO_3$ could well be the most important material for fabrication of devices for commercial usage. But the search for new compounds with superior properties is also on. The salient features of the single phase multiferroic compounds are given here: (i) depending on whether ferroelectric and magnetic orders develop on identical or different sublattice, the entire class of materials is divided into Type-I and Type-II categories [23]; in Type-I systems, the ferroelectric and magnetic order sets in two different sublattices and the transition temperatures—$T_C$ (ferroelectric) and $T_N$ (magnetic)—are also different; the coupling between the order parameters is weak; in Type-II systems, ferroelectric order emerges out of nontrivial magnetic structures (Fig. 4) and therefore, both the transitions are simultaneous; the coupling between the order parameters is large in these cases; (ii) in most of the cases, the origin of ferroelectricity is different; it emerges either from magnetic structure, charge/orbital order, or geometric effect; in these cases, the ferroelectricity is not the primary instability; these systems are called improper ferroelectrics [24]; $BiFeO_3$, $BiMnO_3$, $PbVO_3$ and few other systems, where ferroelectricity is driven by stereochemical activity of A-site ion lone pairs (Fig. 4), exhibit proper displacive ferroelectricity; improper ferroelectric systems exhibit smaller polarization (<1 μC/cm$^2$) whereas the proper ones exhibit large polarization (>10 μC/cm$^2$). It will not be out of place here to mention that from the point of view of applications, composite systems where ferroelectric and magnetic layers form multilayered or other designed structures including one of nanosized columns of one compound embedded within a thin film matrix of another are also quite attractive [25]. The coupling between the order parameters in such composite systems has also been found to be useful for many applications.

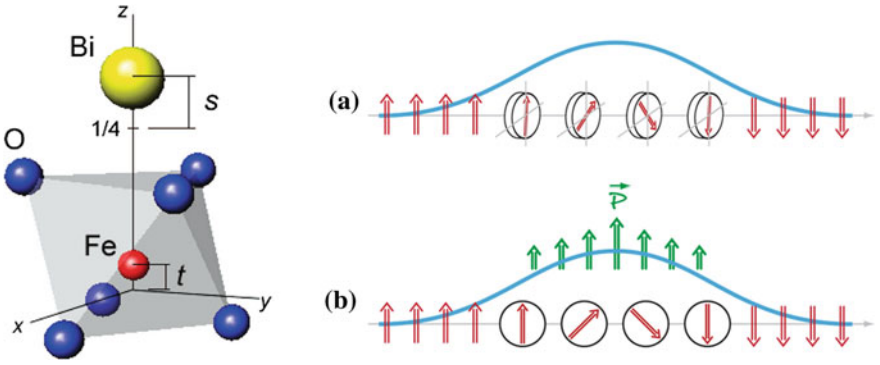


**Fig. 4** The off-centred displacement of Bi and Fe ions along (001) axis in hexagonal setting; right panel shows the spiral spin structure which supports ferroelectricity (one where rotation of spin takes place along its trajectory)

## 3 Energy Efficient Devices Based on Cuprate Superconductors

At the advent of cuprate superconductors, euphoria was generated on the possibility of large scale applications in power transition, storage, generation, and many other electrical and electronic devices. However, it was soon realized that the cuprate superconductors because some intrinsic drawbacks cannot solve the energy crisis by a large scale. Most important drawback is the re-emergence of normal state resistivity with time. Since cuprate systems are Type-II superconductors, magnetic field (generated either by the flowing current itself or from applied external magnetic field) penetrates through the bulk of the sample in the form of quantized vortices. Each vortex line carries one flux quantum $\phi_0 = (h/2e) = 2.015 \times 10^{-15}$ Wb; the core of the vortex (of the size of coherence length $\xi = hv_F/2\pi k_B T_C$) is in normal resistive state while whirlpool of macroscopic current around the core over a length scale of penetration depth ($\lambda$) maintains the flux inside and shields the rest of the superconducting bulk. The vortices start penetrating the bulk of the sample at a lower critical field $H_{c1}(T)$ and fills the entire bulk by the upper critical field $H_{c2}(T) = \phi_0/2\pi\xi^2(T)$, the maximum field at which the superconductivity is retained. While $H_{c1}(T)$ is of the order of 100–500 Oe, $H_{c2}(T)$ is quite large (>1000 kOe). Even though the $H_{c2}(T)$ is large, in practice, superconductivity in the cuprate systems cannot be retained under large magnetic field because of weak pinning force acting on the vortices which make them flow under both thermal activation and Lorentz force. Upon entering the bulk of the sample, the vortices normally follow the crystallographic defects in a sample as these defective regions maintain their normal state (as against superconducting state) and thus offer attractive sites to the vortices. The vortices, therefore, are pinned by the lattice defects. The pinning force is higher than the inter-vortex repulsive force which force them to arrange themselves in a different geometry than the simple hexagonal one predicted by Abrikosov [26] in the absence of lattice defects. Depending on the concentration of the lattice defect (point or line or planar) and vortices within the bulk of the superconductor at a given field, the vortices form many complicated structures including even glassy structure. The magnetic phase diagram, therefore, becomes complicated. More importantly, in presence of flow of current through the sample, Lorentz force $\mathbf{F_L} = q.\mathbf{J} \times \mathbf{B}$ acts on the vortices and if the Lorentz force turns out to be greater than the pinning force $\mathbf{F_p}$—determined by the defect structure of the sample—the vortices start moving which, in turn, gives rise to resistance in the sample. The weak pinning force in the cuprate superconductors also leads to the thermal activation of the vortices because of which normal state resistance emerges over a certain span of time. The vortex flow resistivity, in general, is given by the Bardeen-Stephen formula $\rho = (B/H_{c2})\rho_n$ where $\rho_n$ is the normal state resistivity of a superconductor at above $T_C$. Because of this flux flow, a superconductor looses the superconducting property and becomes resistive even when the operating temperature is well below $T_C$ and the magnetic field is far lower than $H_{c2}$. In fact, detailed study of the magnetic phase diagram and the vortex dynamics under current flow

and thermal activation showed that in cuprate system, the bulk superconductivity is retained up to the irreversibility field $H_{irr}(T)$ which is far smaller than the $H_{c2}(T)$. This is a serious impediment which has prevented cuprate superconductors to be used for large scale applications. The weak pinning force stems from the order of magnitude smaller coherence length $\xi$ (≈10–100 Å; whereas in low-$T_C$ superconductors, it is ∼1000 Å) and also from large anisotropy ($\sim 10^2$–$10^5$). The strength of the thermal fluctuation with respect to the condensation energy of superconductor is expressed succinctly by Ginzburg number $Gi = 2\gamma(k_B T_C m_{ab}/\pi h^2 n \xi^2)$ where $\gamma = m_c/m_{ab}$, m = mass of an electron within ab-plane and along c-axis, and n is the Cooper pair density. In the low-$T_C$ superconductors, the thermal fluctuation is negligible as $Gi \approx 10^{-5}$ to $10^{-6}$ whereas for YBCO system $Gi \approx 10^{-2}$ and for BSCCO system, $Gi \approx 1$. Higher Gi narrows down the operating zone for these cuprate systems within the magnetic field-temperature phase diagram. Another important aspect is the difficulty in fabrication of the cuprate superconducting wires. Because of brittleness, the ceramic cuprate systems cannot be fabricated in the form of wires of cables easily. In spite of this intrinsic shortcoming, power cables as well as superconducting magnets have been developed using cuprate superconducting wires for commercially use. We discuss here the fabrication technique and the devices.

In spite of the above-mentioned shortcomings, during the last decade and a half, tremendous progress has been made in the fabrication of cuprate superconducting cables for power transmission lines and other applications. The first and even second generation cables of $Bi_2Sr_2Ca_2Cu_3O_{10}$ (BSCCO) and $YBa_2Cu_3O_7$ (YBCO) clad within Cu or Ag sheaths are now being fabricated for commercial usage [27] for operating within 20–77 K. This is far above the temperature range at which the Nb–Ti and $Nb_3Sn$ wires (low-$T_C$ superconductors) and the magnets made of them work (<10 K). Insert magnets capable of generating 5T magnetic field within a background of 20T field, generated by Nb–Ti or $Nb_3Sn$ based magnets, have also been developed using the cuprate superconductors. The first generation cables of the cuprate superconductors are fabricated by powder-in-tube (PIT) technique [27] in which superconducting powder is packed inside Ag tube which is then sealed, evacuated, and drawn in the form of a hexagonal rod. The rods are cut and bundled in the form of multifilaments and inserted within a second Ag tube (Fig. 5). This tube is then sealed, evacuated, and drawn in the form of a rod. The rod is rolled in the form of tape with intermediate heat treatment. The superconducting fill factor is typically 30–40%. The filamentary structure of the cables helps in reducing the ac losses. The critical current density ($J_c$) of the cable is measured by allowing more and more current to flow through the sample till a potential drop of 1 μV/cm develops. The corresponding current is called the critical current $I_c$. It is divided by the cross-sectional area of the tape to obtain the 'engineering $J_c$' which is quite useful a parameter for any application. The BSCCO system because of its layered crystallographic structure is amenable for forming flaky textures during processing which reduces the grain boundary misalignment angle (θ). This, in turn, improves the $J_c$ as $J_c$ follows exponential drop with the increase in θ, $J_c \sim J_{c0}.\exp(-\theta/\theta_c)$ [28]. The engineering $J_c$ should attain $10^4$–$10^5$ A/cm$^2$ in magnetic fields 0.1T to

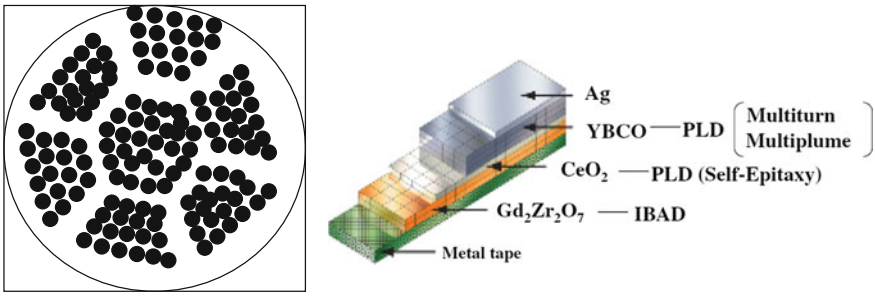


**Fig. 5** The multifilamentary BSCCO2223 wires within Ag sheath in a first generation superconducting cable (after R.M. Scanlan et al. [29]); right panel shows the schematic of the second generation YBCO cable architecture. [S. Tanaka, Jpn. J. Appl. Phys. **45**, 9011 (2006) reproduced with permission from Japan Society for Applied Physics]

25T for applications as power cables and magnets. The actual superconducting $J_C$ is given by $J_c/f$, where $f$ is fill factor. In the case of BSCCO wires, steady progress has been made in improving the $J_c$. It has reached $\sim$ 30,000 A/cm$^2$ at 77 K under 0.1T field. Understanding of the current flow path (the grain colonies which allow the current flow unhindered) and the role of the defects in pinning the vortices and improving the current carrying cross-section of the superconducting filament helps in designing the cables better.

The second generation cable technology [29] uses multiple processing routes comprising of epitaxial thin film deposition on tape-shaped templates (Fig. 5). This epitaxial texture is then replicated to form the YBCO wires with high degree of grain alignment. YBCO system with lower anisotropy and consequently higher $H_{irr}(T)$ offers higher operating temperature than BSCCO.

These first and second generation cables of BSCCO and YBCO superconductors find applications in power transmission lines, power equipment, motors, generators, synchronous condensers, transformers, and fault-current limiters for the electric utility grid.

Alongside all these, applications of cuprate superconductor based Josephson junctions are also envisaged as superconducting quantum interference device (SQUID) sensors working at 77 K. In a SQUID, single or double Josephson junctions are introduced within a superconductor circuit through which superconducting current tunnels. The circuit current changes significantly under application of a magnetic field. The magnetic field attaches to the device in the form of quantized fluxes ($\phi = n\phi_0$). The change in current, in turn, is used to measure the applied field and also magnetization of a sample. Because of substantial change in the tunnelling current under even one flux quantum $\phi_0$ (= 2.07 $\times$ 10$^{-15}$ Wb), a SQUID sensor is extremely sensitive.

A SQUID prepared by using Josephson junction of YBCO system (by depositing thin film of YBCO on a bicrystal to introduce the Joesphson junction) works at 77 K and has been used for magnetocardiography. Hitachi Ltd. has developed [30] an array of 51 SQUIDs for studying the human heart diseases. Of

course, the sensitivity of YBCO based SQUIDs working at 77 K is about ten times lower than Nb based SQUIDs working at 4 K. An array of Josephson junctions comprising of 100 junctions with YBCO superconductors are used [31] for constructing single quantum flux (SFQ) device (Fig. 6). In this device, the quantized magnetic field under application of short pulse of current can either appear or disappear and thus render the junctions normal or superconducting. The state of the flux is designated as '0' or '1'. The combination of generation of quantized flux and its transmission by Josephson transmission line is used for many logic operations. These logic operations use just 0.1 μW of power which is 100 times smaller than any semiconductor based logic gate device. The operation speed, on the other hand, is 100 times faster. The YBCO based SFQ devices are capable of working at 40 K.

In summary, cuprate superconductors are continuously pushing the boundary and increasingly find applications in large and small scale electrical and electronic devices. With the improvement of materials processing technology, problem of weak pinning of magnetic flux lines (vortices), brittleness of the ceramic systems, stability of the persistent mode operation, relatively low operating temperature than what was envisaged at the beginning are being solved. Great future awaits the cuprates in many diverse fields, glimpses of which have been presented here.

## 4 Energy Efficient Devices Based on Magnetoresistive Manganites

Large negative magnetoresistance in magnetic multilayer (comprising of two metallic magnetic layers sandwiching a nonmagnetic metallic layer) and spin valve effect opened the door of spintronics or spin-based electronics where spin of an electron (instead of charge) is used for transmission and processing of information. The spin transport with larger coherence length and precession time helps in enhancing the efficiency of information storage and communication. The

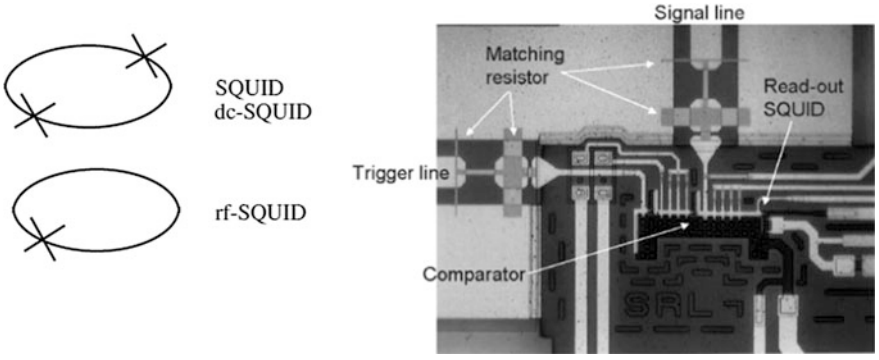


**Fig. 6** The schematic of one and two Josephson junction SQUID and (right panel) the image of a sampler device associated with SFQ. [S. Tanaka, Jpn. J. Appl. Phys. **45**, 9011 (2006) reproduced with permission from Japan Society of Applied Physics]

observation of orders of magnitude decrease in electrical resistance under magnetic field in perovskite manganites ($RMnO_3$ with doping by Ca, Ba, or Sr at R-site) has created new possibilities for spintronic devices. The magnitude of magnetoresistance in doped perovskite manganites is even larger than what is observed in metallic magnetic multilayers. The charge carriers in manganites are almost 100% spin polarized (large band gap develops between up and down spins) with either up or down spins flowing through the sample [32]. These materials, therefore, are called half metals. The extent of spin polarization is given by $P = [N_{\uparrow}(E_F) - N_{\downarrow}(E_F)]/[N_{\uparrow}(E_F) + N_{\downarrow}(E_F)]$ where $N(E_F)$ is the density of electron states with either up or down spin – as the case may be—at the Fermi level ($E_F$). This is utilized in spin polarized magnetic tunnel junction devices.

The magnetic tunnel junctions (MTJ) are used for non-volatile magnetic random access memories (MRAM) (Fig. 7) which are superior to the dynamic random access memories (DRAM) and static random access memories (SRAM). The DRAM and SRAM systems are volatile because of leakage currents in the circuit. They need to be refreshed by frequent power supply. The MRAMs, on the other hand, do not require frequent power supply. The MTJs are constructed from two ferromagnetic electrodes and a thin tunnel barrier with fully spin polarized currents flowing across the tunnel barrier. One of the electrodes is pinned while the other is left free for the applied magnetic field to align the spins. Depending on whether the spins are aligned in parallel or antiparallel in the electrodes, spin-polarized current can flow with minimum or maximum tunnel resistance. The tunnelling magnetoresistance (TMR) is given by $2P_1P_2/(P_1 + P_2)$ where $P_1$ and $P_2$ are the spin polarizations in the two ferromagnetic electrodes. Because of nearly 100% spin polarization in $La_{0.7}Sr_{0.3}MnO_3$, the TMR is very large under moderate magnetic field. This is utilized in MRAM devices [33]. Similar effect can also be observed within a ferromagnetic layer by engineering a domain wall or defect line

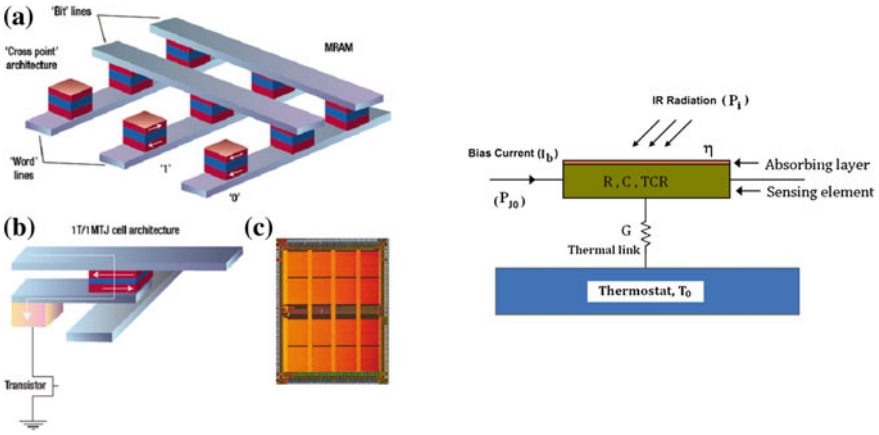


**Fig. 7** Schematic of MRAM device based on magnetic tunnel junctions and also a photograph of the real device is shown in (**c**); right panel shows the schematic of the bolometer device

(grain boundary) across which the spins are rotated [34]. For perfect spin alignment across that nano-constriction, the resistance is small whereas the resistance become large for anti-alignment of the spins across the constriction. Under moderate magnetic field, the spins are aligned across the constriction giving rise to large magnetoresistance.

Another important manganites based device is the IR detector or bolometer (Fig. 7). Since the temperature coefficient of resistance (TCR) around the metal-insulator transition is large in this class of compounds, they are suitable for bolometers [35]. The typical response time is of the order of few ns which is fast enough for practical applications. The sensitivity and noise (due to fluctuations in incident energy, Johnson and phonon noise in the circuit) in the circuit could be defined in terms of normalized Hooge parameter. Large TCR and small Hooge parameter are suitable for bolometer application. Because of metal-insulator transition taking place near room temperature in $La_{0.7}Sr_{0.3}MnO_3$, this compound is suitable for room temperature bolometer devices in spite of relatively smaller TCR here than other manganites such as $La_{0.7}Ca_{0.3}MnO_3$.

The colossal magnetoresistive manganites find applications is the magnetoresistive read heads of the magnetic data storage medium. Sharp change in electrical resistivity under tiny magnetic field—observed in CMR systems—is exploited for reading a magnetic bit stored in a medium of nanosized domains. With such read heads, the data storage density enhances manyfold than conventional inductive head where current is induced in the head in the vicinity of magnetic storage medium. The CMR manganites are expected to achieve as high a storage density as 1 Tbit/in$^2$. Of course, the intrinsic magnetoresistance in the manganites is colossal only under a higher field (of the order of 1 to 2T) whereas for read head application, large magnetoresistance should be observed under few tens of Oersted. This is achieved in granular CMR system where spin polarized intergranular transport exhibits large magnetoresistance under low field. The granular structure is developed [36] by artificially etching out grain boundaries in thin film of CMR oxide (Fig. 8).

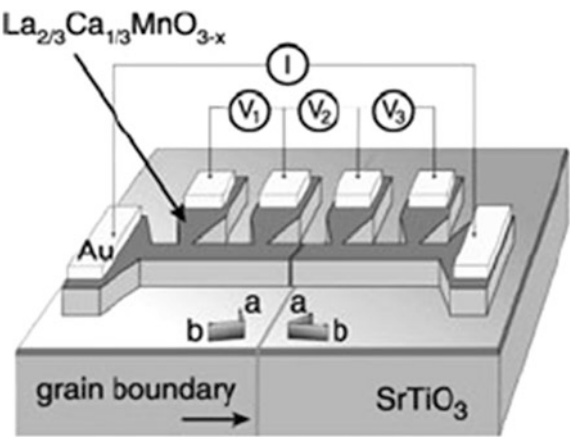


**Fig. 8** Schematic of artificially etched grain boundaries in a thin film of CMR manganite

While CMR of the manganites—being exploited in MRAM, disk read head, and bolometer devices—are observed in the composition regime where the sample assumes ferromagnetic and metallic properties, the regime where long-range charge/orbital order prevails and the sample exhibits primarily antiferromagnetic and insulating behaviour is also suitable for novel spin and orbital based electronic applications. Importantly, because of closeness of the energy scales involved, the interplay among charge, spin, orbital, and lattice degrees of freedom is quite delicate in different regions of the phase diagram and this, in turn, can be exploited by switching the ordered states or order-disorder transition under external stimulation such as light pulse, electric or magnetic field. In a charge/orbital ordered system, electrons occupy specific d-orbitals which, in turn, organize in different patterns; electrons, therefore, carry their orbital degrees of freedom in such cases. Because of associated polarizability, the orbital degree of freedom couples with the applied electric field and/or optical pulse. It has been demonstrated [37, 38] that ultrafast switching of orbital states (as the orbitals and their dynamic response 'orbitons' have a typical response frequency 10–100 THz which is orders of magnitude larger than 0.1–1.0 GHz spin precession frequency) and/or melting under optical pulse can be utilized in optical devices (Fig. 9).

In summary, CMR manganites find applications as MRAM, magnetic disk read head, bolometer, and also orbitronic devices where melting of orbital order gives rise to gigantic change in physical properties such as resistivity, magnetization, thermal properties, optical constants etc. which recover slowly with time. Such changes can be utilized for ultrafast optical switches.

## 5 Energy Efficient Devices Based on Multiferroics

The spin and orbital based electronic devices receive a boost from the multiferroics where coexisting ferroelectric and magnetic order and their coupling expands the horizon even further. The advantages of FeRAM and MRAM can now be

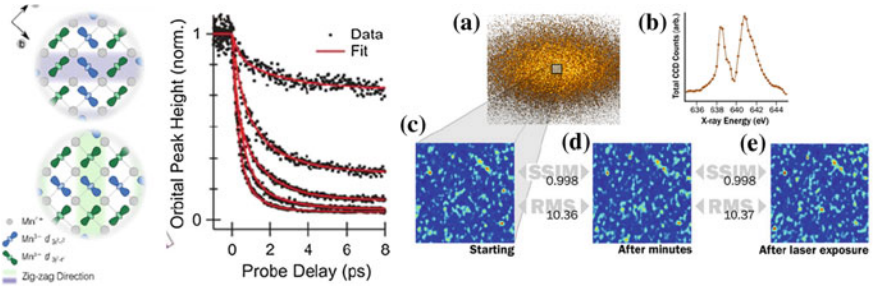


**Fig. 9** Orbital domain structures with two different types of Mn 3d orbital patterns; the peak corresponding to the orbital order in $La_{1.8}Ba_{0.2}MnO_4$ melts rapidly under laser fluence of 60 mJ/cm$^2$within 1–2 ps; right panel, however, shows that over a time span of few minutes the orbital order recovers fully with virtually identical speckle patterns [*source* https://upcommons.upc.edu/bitstream/handle/2117/107059]

integrated into a single multiferroic memory device which offers four independently accessible logic states [(+P, +M), (+P, −M), (−P, +M), and (−P, −M); where P and M are polarization and magnetization, respectively] – not possible to access in FeRAM or MRAM separately—and consequently exponentially enhanced computation capacity. The voltage driven multiferroic memory because of very small current flow requires an order of magnitude smaller power supply and also exhibits an order of magnitude smaller Joule heating than spin torque transfer type memories which depend on spin polarized current flow.

The major bottleneck, however, is the non availability of suitable multiferroic compound which exhibits ferroelectric and ferromagnetic orders and strong cross-coupling at room temperature itself. Very recently, of course, epitaxial thin film based device of room temperature multiferroic $BiFeO_3$ was shown to exhibit complete 180° switching of magnetic domains under electric field [39]. Energy consumption in such a device was shown to be $\sim$0.5 mJ/cm$^2$ which is nearly an order of magnitude smaller than the energy consumption of a spin torque transfer type memory ($\sim$3–4 mJ/cm$^2$). This device or, alternately, where multiferroic $BiFeO_3$ and ferromagnetic $La_{0.7}Sr_{0.3}MnO_3$ (LSMO) are formed as multilayers, exchange coupled device (Fig. 10) could well be used as real-life multiferroic memory in near future [40]. In the exchange coupled device, the magnetic anisotropy of the ferromagnetic LSMO layer was shown to switch under electric field because of switching of anisotropy in $BiFeO_3$ under electric field and exchange coupling between antiferromagnetic $BiFeO_3$ and ferromagnetic LSMO which generates sizable exchange bias field at the interface.

The non-availability of single phase room temperature multiferroic has been circumvented by multilayers of ferroelectric ($BaTiO_3$) and ferromagnetic ($La_{0.7}Sr_{0.3}MnO_3$) systems which exhibits nearly 400% large tunnelling magnetoresistance [41]. This system also works as low energy memory device. Similar

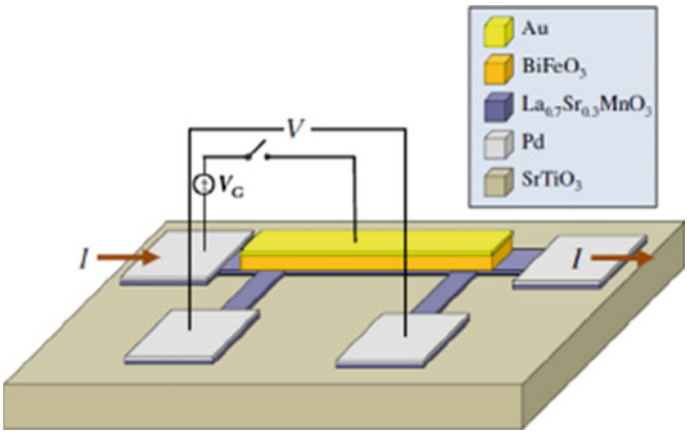


**Fig. 10** Schematic of the exchange coupled multiferroic memory device comprising of $BiFeO_3$ and $La_{0.7}Sr_{0.3}MnO_3$ layers

device has been developed by using $PbZr_{0.52}Ti_{0.48}O_3$(PZT)/$La_{0.7}Sr_{0.3}MnO_3$ (LSMO). The heteroepitaxy, in fact, is currently the main theme underlying the device configuration for multifunctional device development. Heterostructures of $Co_{0.9}Fe_{0.1}/BiFeO_3$ and $BaTiO_3/BiFeO_3$ have also been developed [42] for memory and magnetoelectric sensor applications.

The piezoelectric effect and magnetoelectric coupling in composite ferroelectric/magnetic system have been used [43] for magneto-mechano-electric generator. Multilayers of PMN-PZT ferroelectric, Ni magnetostrictive, and Nd magnetic systems with Cu electrodes laminated within are used to generate as high as ~9.5 V under $H_{ac}$ of 160 mT (at 60 Hz) without any dc external magnetic field. The power density appears to be ~46.3 $mW/cm^3/Oe^2$ which is ~1600% higher than conventional devices. This device can be used as power source for wireless sensor network, low power electrical devices, and wireless charging system.

The composite of magnetic and ferroelectric systems, in fact, were shown to be useful for a variety of other low power device applications such as microwave resonator, phase shifter, delay line. The yttrium iron garnet (YIG) and PZT composite has been used [44] to demonstrate the tuning of ferromagnetic resonance (FMR) in the YIG, driven by electric field, at a signal input of 2–10 GHz and 0.1 mW power. The resonance frequency shifts from 5 GHz under zero electric field by +16 MHz under +10 kV/cm and −18 MHz under −10 kV/cm. The use of electric field as against magnetic field in all these cases reduces the power consumption by a large extent.

Single phase multiferroic systems find applications even as photovoltaic cell based devices. In a photovoltaic cell, irradiation of sunlight creates electron-hole pairs by exciting the electrons across the band gap in a semiconductor which, in turn, are separated for producing the current flow in the circuit. Normally, this is achieved in a p-n junction device. The semiconductor of small band gap absorbs more photons and creates large current while the one of large band gap absorbs lesser photons and creates large voltage. Striking a balance between the two is a problem. This requires bulk photovoltaic effect instead of the one observed at the p-n junction interface. Bulk photovoltaic effect is observed in ferroelectric systems where additional internal electric field due to large ferroelectric polarization (P) helps in photocurrent flow [45]. This, in turn, offers larger open circuit voltage than what is observed in p-n junction device. However, one disadvantage of the ferroelectric cell is large band gap (of the order of 3–6 eV) which prevents entire solar light spectrum to be used. Single phase multiferroics such as $BiFeO_3$ with relatively smaller band gap (~2.3 eV) or double perovskite $Bi_2CrFeO_6$ (band gap ~1.4–2.0 eV) appear to be suitable for photovoltaic cells [46]. It has been argued that exchange coupling interaction associated with long-range magnetic order is responsible for reducing the band gap. The switching of ferroelectric polarization and/or turning it on by external magnetic field—as is possible in a multiferroic system—make them more attractive. The schematic of the function of a multiferroic based solar photovoltaic cell is shown in Fig. 11. The coupling among strain-ferroelectric-magnetic properties makes the multiferroics extremely attractive for photovoltaic application.

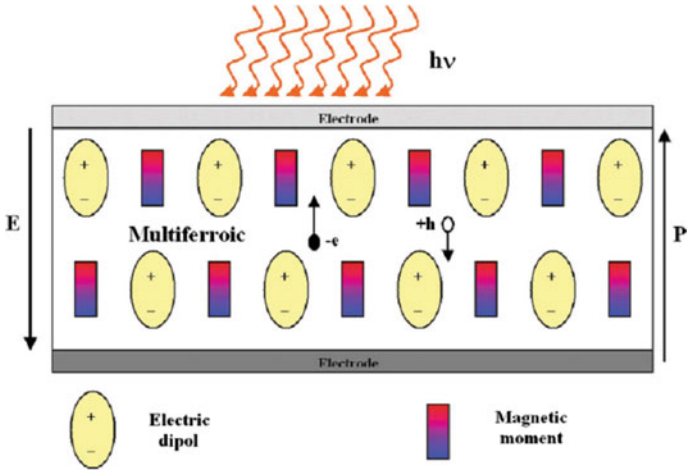


**Fig. 11** Schematic of bulk photovoltaic effect in multiferroic system in presence of electric and magnetic dipoles

An extremely important upcoming application of multiferroic systems is in the biomedical field. Here, rectification of a faulty ion channel could be carried out by insertion of a nanoscale multiferroic device. This device generates electric field locally—thus operates the ion channel valves—under remote application of magnetic field [47]. The two main characteristics of the ion channels are their selectivity and their gating (process of opening and closing in response to gating variable). In the recent past, researchers have focussed on the effect of electric field on these ion channels using currently available multiferroic nanoparticles. Though it is a well accepted fact that the function of ion channel can be modified through the use of drugs, the prospect of multiferroic nanoparticles is worthy of detailed investigation. In some of the recent papers, it is reported that multiferroic particles introduced extra or intra-cellularly can modify the electric field and control ion channel gating by externally applied magnetic fields. Therapeutic use of electric or magnetic field till date has its own limitations. It includes use of high voltage (sometimes above 200 volts), exposure to large volume of tissues, direct contact with body fluids in case of percutaneous electrodes etc. In case of multiferroic composites, individual cells are proposed to be targeted, not the whole tissue. The voltage required for the stimulation is also reported to be in millivolts. Moreover cell functioning in internal organs can be controlled in a remote way. When an external magnetic field is applied, the multiferroic particles can convert it to localised electric field. If the particles are placed near cell membranes, this may lead to membrane depolarisation and accordingly, the ion channels can open. The magnetic field can be applied globally by the Helmholtz coils but the electric field will still be locally generated. This will lead to localised changes in ion channel gating. Moreover, it is also interesting that the signals generated by nanoparticles have closely similar characteristics to those of electric signals propagating in neural cells. In future, it can

generate new scopes to remotely stimulate the functions of neural cells for pain management. Another important issue arising out of the use of multiferroic composites is the scope of applying magnetic field pulses with higher frequencies. The ion channels may not respond to high frequency fields, but the strength of electric fields produced by the multiferroic nanoparticles may be sufficient to cause electroporation of cell membranes and cause permanent damage which, in turn can provide a tool for cancer treatment.

In summary, a variety of spintronic based devices are possible for either single phase or composite multiferroic systems ranging from four-logic-state next generation memory, to read heads, to sensors, tunable resonators, magneto-mechano-electric generators, photovoltaic cells to even biomedical implants. In all the cases power consumption and efficiency of the devices appear to be lot better than the conventional devices.

## 6 Future Projection

In the previous paragraphs, glimpses of the developments made in the area of 'strongly correlated electron system' based electronic, spintronic, and orbitronic devices have been given. In spite of the great promise of the cuprate superconductor, CMR manganite, and multiferroic compounds, it is true that many issues still need to be solved in order to go for full scale commercial usage. Some of the issues are intrinsic such as giant vortex creeping in cuprates which destroys superconductivity in the long run, non-availability of single phase multiferroic system exhibiting ferroelectric and ferromagnetic properties as well as large magnetoelectric coupling right at room temperature. Some of the issues, however, are operational. For instance, interesting properties could be observed in laboratory scale on thin films prepared on single crystal substrates by sophisticated techniques such as pulsed laser deposition. However, for industrial processing low-cost chemical vapour deposition or sputtering technique and cheaper substrates are required. The heteroepitaxy, currently being explored for artificially building up novel device architecture [48] capable of exhibiting requisite functionality, needs to be simple and cheap enough to be industrially viable. While, technological development at the laboratory scale such as molecular beam epitaxy, laser based synthesis, atomic force microscopy based tailoring can certainly yield novel material properties by ingenuous lattice strain/defect engineering, greater ingenuity is required to achieve the same result in rather simple and cheaper techniques. The development of novel industrially viable processing technique appears to be a major bottleneck for commercial use of these systems.

However, as discussed above, the prospect of the 'strongly correlated electron systems' is certainly bright and in near future with the advancement in material processing technology, commercial devices will roll out for ushering in an era of 'strongly correlated electron' system based electronics.

One of the authors (SG) acknowledges Senior Research Associate-ship of CSIR, Govt of India during this work.

## References

1. Bednorz JG, Muller KA (1986) Z Phys B 64:189
2. See, for example, Dagotto E (1994) Rev Mod Phys 66:763
3. See articles in *Colossal Magnetoresistance, Charge Ordering, and Related Properties of Manganese Oxides*, edited by C.N.R. Rao and B. Raveau (World Scientific, Singapore, 1998)
4. Wang KF, Liu J-M, Ren ZF (2009) Adv Phys 58:321
5. See, for example, Chappert C, Fert A, Van Dau FN (2007) Nat Mater 6:813
6. Cox DL, Maple MB (1995) Phys Today 48(2):32
7. Anderson PW (1997) The theory of high-$T_c$ superconductivity. Princeton University Press, Princeton
8. Wu MK et al (1987) Phys Rev Lett 58:908
9. Maeda H et al (1988) Jpn J Appl Phys 27:L209
10. Tarascon JM et al (1988) Phys Rev B 38:8885
11. Mott NF, Davis EA (1971) Electronic processes in non crystalline materials. Clarendon Press, Oxford
12. Maeda A et al (2005) J Phys: Condens Mater 17:143
13. Tahir-Kheli J, Goddard WA (2010) J Phys Chem Lett 1:1290
14. Blatter G et al (1994) Rev Mod Phys 66:1125
15. Eshurum Y et al (1996) Rev Mod Phys 68:911
16. Jin S et al (1994) Science 264:413
17. See the articles in Colossal Magneto-resistive oxides, edited by Y. Tokura (Gordon and Breach, Amsterdam, 2000)
18. See for example, Dagotto E et al (2001) Phys Rep 344:1
19. Tomioka Y et al (1995) Phys Rev Lett 74:5108
20. Filipév VS et al (1961) Sov Phys Crystallogr 5:913
21. Hill NA (2000) J Phys Chem B 104:6694
22. Wang J et al (2003) Science 299:1719
23. See for example, Khomskii D (2009) Physics 2:20
24. Cheong SW, Mostovoy M (2007) Nat Mater 6:13
25. Zheng H et al (2004) Science 303:661
26. Abrikosov AA (1957) Sov Phys JETP 5:1774
27. Larbalestier DC et al (2001) Nature 414:368
28. Gurevich A, Pashitskii A (1998) Phys Rev B 57:13878
29. See for example, Scanlan RM et al (2004) Proceedings of the IEEE, vol 92, p 1639
30. Tsukamoto A et al (2005) IEEE Trans Appl Supercond 15:173
31. Suzuki H et al (2005) Physica C 426–431:1643
32. Bowen M et al (2003) Appl Phys Lett 82:233
33. See for example, Wolf SA et al (2007) Science 294:1488
34. Bruno P (1999) Phys Rev Lett 83:2425
35. Kim J-H et al (2003) Appl Phys Lett 82:4295
36. Mathur ND et al (1997) Nature 387:266
37. Singla R et al (2013) Phys Rev B 88:075107
38. Miller T, Gensch M, Wall S (2016) Phys Scr 91:124002
39. Heron JT et al (2014) Nature 516:372
40. See for example, Heron JT et al (2014) Appl Phys Rev 1:021303
41. Lorenz M et al (2016) Adv Mater Interfaces 3:11500822

42. Heron JT et al (2011) Phys Rev Lett 107:217202
43. Ryu J et al (2015) Energy Env Sci 8:2402
44. Fetisov YK, Srinivasan G (2006) Appl Phys Lett 88:143503
45. Glass AM et al (1974) Appl Phys Lett 25:233
46. Nechache R et al (2011) Appl Phys Lett 98:202902
47. Kargol A et al (2012) In: Malkinski L (ed) Advanced magnetic materials. In Tech, Rijeka, Chapter 4
48. See for example, Lorenz M et al (2016) J Phys D: Appl Phys 49:433001